

# On the Exchange of Carbon Dioxide between Atmosphere and Ocean

John Reid

## Key Points:

- The atmosphere exchanges CO<sub>2</sub> with both the mixed layer and the deep ocean.
- The impulse response function of CO<sub>2</sub> concentration estimated from observations has a half-time of 43 years and no remnant fraction.
- Impulse response functions determined by numerical modelling are not supported by observations.

---

Corresponding author: John Reid, [johnreid2844@gmail.com](mailto:johnreid2844@gmail.com)

**Abstract**

There are two distinct reservoirs which exchange carbon with the atmosphere, the mixed layer and the deep ocean. Exchanges with the former are noisy because they are influenced by sea surface temperature which, in turn, depends on weather events such as El Niño. Exchanges with the deep ocean are steady, long-term and uninfluenced by the weather. The long term relationship between CO<sub>2</sub> concentration due to variations in CO<sub>2</sub> emissions is summarised by the Impulse Response Function. This was estimated from observed time series as the convolutional inverse of the prediction error filter estimated by the ARX method. It was found to be a simple exponential with a half-time of 43 years and no remnant component. The longer half times and large remnant fraction of the impulse response derived from ocean circulation models are attributed to the failure of these models to properly account for turbulent mixing in the deep ocean.

**Plain Language Summary**

Carbon dioxide in the atmosphere is exchanged rapidly with the upper part of the ocean, the mixed layer. When the temperature of the mixed layer increases, as it does in the Pacific Ocean during El Niño events, concentration in the atmosphere briefly increases. On the other hand, radioactive carbon dioxide from the atom bomb tests steadily disappeared from the atmosphere once the tests had stopped in 1963, implying that it was absorbed by the deep ocean below the mixed layer. The relationship between carbon dioxide production and concentration can be summarised mathematically by the impulse response function or IRF which is used in climate models to predict future concentrations. We developed a new method of estimating the IRF directly from the data. This, the observed IRF, is quite different from the IRF used by climate modellers in that no carbon dioxide is left behind to build up over centuries. Climate modellers might make better predictions if they used this observed IRF.

**Keywords**

carbon cycling, Impulse Response Function, ARX method, convolutional inverse, remnant fraction.

**AGU Index Terms**

carbon cycling 4806, 3339 Ocean/atmosphere interactions (0312, 4301, 4504), 3270 Time series analysis (1872, 1988, 4277, 4475), 1968 Scientific reasoning/inference, 1986 Statistical methods: Inferential (4318)

**1 Introduction**

Information about the interchange of carbon between various global sinks and reservoirs can be found in the IPCC reports (Houghton et al., 2001). Much of this is stated *a priori* as the outcome of various model assumptions. Here we adopt an empirical approach and investigate atmospheric CO<sub>2</sub> concentration in the context of concurrent natural and man-made forcing. One such is El Niño and the increased sea surface temperature (SST) of the Eastern Equatorial Pacific which accompanies these events. Another is the testing of nuclear weapons during the 1950s and 1960s which injected significant amounts of the radioactive isotope of carbon into the atmosphere as <sup>14</sup>CO<sub>2</sub>. The abrupt cessation of atmospheric testing following the Nuclear Test Ban Treaty of 5 August 1963, meant that the rate of production of the <sup>14</sup>C isotope reverted to the constant natural background level. This allows the movement of carbon dioxide between reservoirs to be assessed in much the same way that radioactive isotopes are used to assess the rates of metabolic processes in nuclear medicine.

Most importantly, the relationship between CO<sub>2</sub> production and the resulting atmospheric concentration needs to be better understood. Such a relationship between time series (or continuous functions) of physical quantities is succinctly summarised by the Impulse Response Function (IRF) which displays how the dependent variable will respond to a discrete impulse (or delta function) in the independent variable. This can often be estimated by numerical modelling of the physical processes underlying the relationship between the variables, for example, by Maier-Reimer & Hasselmann (1987) (MRH) as discussed below.

Alternatively it can be estimated from the data statistically. This is, however, a notoriously difficult problem (Riad, 1986), involving as it does, the deconvolution of a moving average (MA) process. Here we circumvent the difficulties of MA processes in two ways:

- (i) by decimating the data to remove the blurring effect of the moving average and
- (ii) by estimating the statistically significant coefficients of the prediction error filter (PEF) via the ARX method. The normalized IRF is then the convolutional inverse of the PEF.

The IRF estimated in this way is less complex and differs significantly from that of MRH.

## 2 El Niño

Values of the first differences of the monthly average concentration measured at the Cape Grim and Mauna Loa observatories are shown in Figures 1a and 1b respectively. Thirteen month running means are also shown. There is a significant linear trend in both time series. The standard deviations,  $\sigma$ , of the residuals were 0.14 and 0.30 ppm/month respectively. The dashed lines show the  $2\sigma$  confidence limits above and below the trend lines.

Figure 1c shows the Southern Oscillation Index for the period in question. The SOI is calculated from the sea level pressure difference between Tahiti and Darwin. Sustained negative excursions of the SOI are termed El Niño events and are associated with increases in Sea Surface Temperature in the Eastern Equatorial Pacific as shown in Figure 1d for the Niño3 region, 5°N-5°S, 150°W-90°W (Trenberth, 1997). The times of these SST peaks in Figure 1d are shown by vertical dashed lines in all four panels.

All four El Niño warming events are associated with increases in the running means of atmospheric CO<sub>2</sub> concentration at both Cape Grim and Mauna Loa. This is not surprising. The solubility of CO<sub>2</sub> in sea water is inversely dependent on temperature and it comes out of the ocean when SST increases. In general, the high frequency noisiness of the monthly differences can be accounted for by the degassing and absorption of CO<sub>2</sub> by the upper part of the ocean as it is heated and cooled by changing weather systems.

## 3 The Bomb Test Curve

The decrease in  $\Delta^{14}\text{C}$  is known as “The Bomb Test Curve”. Numerous observations were made in the decades following the cessation of testing following the Nuclear Test Ban Treaty. Here we look at a single high quality data set from Fruholmen, Norway (Nydal & Lövseth, 1983) shown in Figure 2. The natural logarithm,  $\ln(\Delta^{14}\text{C})$ , is plotted on the vertical axis rather than  $\Delta^{14}\text{C}$  itself so that exponential behaviour becomes linear.

A regression line was fitted between January 1966 and the end of the data set in June 1993. Regression statistics are shown in Table 1. The fit is remarkably good and accounts for 98.8 percent of the variance. Hence, with a high degree of accuracy:

$$\Delta^{14}\text{C} = Ae^{-t/\tau} \tag{1}$$

where  $A$  is the value of  $\Delta^{14}\text{C}$  at  $t = 0$  and  $\tau$  is the time constant given by  $\tau = -1/\text{slope} = 15.9 \pm 0.085$  years. The time for  $\Delta^{14}\text{C}$  to decay to half its initial value is given by  $t_{1/2} = -\tau \ln(0.5) = 11.02 \pm .059$  years.

Thus half of the bomb test  $^{14}\text{CO}_2$  disappears from the atmosphere every 11 years. Equation (1) is the solution of the classic diffusion equation:

$$\frac{dc}{dt} + \frac{c}{\tau} = F(t) \quad (2)$$

where  $c$  is the concentration of the quantity being diffused ( $\Delta^{14}\text{CO}_2$  in this case),  $\tau$  is the diffusion time constant and  $F(t)$  specifies the rate at which concentration increases due to new material being introduced into the reservoir. In this case following the cessation of nuclear testing  $F(t)$  is the constant background rate associated with the bombardment of upper atmosphere Nitrogen by cosmic rays.

Carbon dioxide reacts with water to form carbonate and bicarbonate ions. Hence the diffusion rate of carbon *per se* involves reaction rates and diffusion rates for each of these three species. These are almost completely independent of atomic mass Zeebe (2011) and so all the isotopes of carbon,  $^{12}\text{C}$ ,  $^{13}\text{C}$ ,  $^{14}\text{C}$ , in the form of  $\text{CO}_2$  and its radicles, diffuse through water at the same rate and the time constant,  $\tau$ , in (2) applies equally to all isotopic species of  $\text{CO}_2$ .

It is therefore reasonable to assume that  $\text{CO}_2$  diffuses from the atmosphere into some other reservoir or sink. The excellent fit of a single regression line indicates that any diffusion process must be dominated by a single sink with a single time constant. Furthermore the fact that the atmospheric  $\Delta^{14}\text{CO}_2$  has, by now, returned to its pre-bomb background level implies that the sink is much larger than the source, the atmosphere. The only candidate sink which fulfils these conditions is the deep ocean. Note that the half time for  $^{14}\text{CO}_2$  diffusion out of the atmosphere of 11 years is much smaller than the value of 43 years derived below. Unlike in the latter case, radioactive tracer diffusion is a one way process because there is no  $^{14}\text{CO}_2$  simultaneously diffusing back into the atmosphere

## 4 The Impulse Response Function

The impulse response function or IRF,  $I$ , once known, is a great convenience for modellers because it allows an endogenous quantity,  $y(t)$ , to be predicted in terms of present and past values of the exogenous quantity,  $x(t)$ , using the convolution

$$y(t) = \int_{-\infty}^{\infty} I(t')x(t-t')dt' = \int_0^{\infty} I(t')x(t-t')dt' \quad (3)$$

since  $I(t') \equiv 0$  for  $t' < 0$ . For display purposes, a normalized IRF,  $\mathfrak{S}$ , is often used where

$$y(t) = \int_0^{\infty} \mathfrak{S}(t')\chi(t-t')dt' \quad (4)$$

and  $\chi(t)$  has been scaled to have the same units as  $y(t)$ .

In the following,  $y(t)$ , is the atmospheric  $\text{CO}_2$  concentration and  $x(t)$ , is the  $\text{CO}_2$  emission rate.

### 4.1 The Model-Derived IRF

A normalized IRF  $\mathfrak{S}(t)$  was derived using a global circulation model by MRH, assuming

$$\mathfrak{S}(t) = A_0 + \sum_{j=1}^4 A_j \exp(-t/\tau_j) \quad (5)$$

where the  $A_j$  are the proportions corresponding to various decay times,  $\tau_j$ . They found time constants,  $\tau_j$  ranging from 1.2 years to 362.9 years and that  $A_0$  is non-zero. A very similar model, the HILDA model, was proposed by Siegenthaler & Joos (1992) which ultimately became the Bern model of the IPCC reports.

In order to assess the non-linear response of pCO<sub>2</sub> to total carbon in the mixed layer, MRH ran their model using three input emission scenarios comprising increases of (a) quadrupling, (b) doubling and (c) increasing by 1.25%, the initial atmospheric CO<sub>2</sub> concentration. Values of  $A_0$  were 0.131, 0.166 and 0.142 respectively which determine the remnant fractions of atmospheric CO<sub>2</sub> under the three scenarios.

There is something very odd about this. Certainly we might expect a remnant fraction to remain in the atmosphere once the oceanic reservoir is saturated. What is odd is that the three remnant fractions are almost the same. In each case, we would expect the reservoir to take up roughly the same *absolute* amount of CO<sub>2</sub> before it becomes saturated, in which case a twice the *fraction* would remain in the atmosphere in the quadrupling case than in the doubling case, but this is not what happens to the dotted curves in Figure 3.

The similarity of the remnant fractions in the three cases does not imply saturation. Rather, it implies a partitioning of the available CO<sub>2</sub> between two reservoirs with a volume ratio of the order of  $(1 - r)/r$ , where  $r$  is the remnant fraction. When we apply this to the MRH model, the oceanic reservoir into which atmospheric CO<sub>2</sub> is diffused has only about six times the CO<sub>2</sub> capacity of the atmosphere. Given that the ocean has been estimated to carry fifty times the steady-state, atmospheric load of CO<sub>2</sub> (Houghton et al., 2001), this is a remarkably small value. It implies that, in the MRH model, CO<sub>2</sub> becomes partitioned between the atmosphere and a small sub-reservoir from which little is absorbed into the remainder of the ocean.

## 4.2 Estimating the IRF from Observed Time Series

For notational convenience, in the following, all sample means have been removed and random variables are assumed to have zero mean.

The autoregressive moving average method with a single exogenous variable, ARMAX( $p,q$ ), is given at time,  $i$ , by:

$$Y_i = \alpha_0 x_i + \sum_{j=1}^p \alpha_j \cdot y_{i-j} + \sum_{k=1}^q \beta_j \Xi_{i-k} \quad , \quad i = 1, \dots, N \quad (6)$$

where the dependent random variable is  $Y_i$ ,  $x_i$  is the exogenous variable, the  $y_i$  are past values of  $Y_i$  and the  $\Xi_i$  are unselfcorrelated random variables with zero mean. The regression coefficients  $\alpha_0$ ,  $\alpha_j$  and  $\beta_j$  are estimated from the data and  $p$  and  $q$  are small positive integers. The notation is intended to make a clear distinction between random variables which are upper case, and constants, such as past values of random variables, which are lower case. Equation (6) is a state space representation (Hamilton, 1994) describing states of the system at a succession of discrete instants; the random variable,  $Y_i$ , at one instant becomes the constant,  $y_i$ , in the following instant. The direction of time is important in regression, which, unlike correlation, allows causality to be inferred (Granger, 1969).

There are software packages for ARMAX parameter estimation available under the aegis of the major programming languages. Unfortunately some of these are flawed, because they estimate the exogenous parameter,  $\alpha_0$ , prior to estimating the other parameters, leading to omitted-variable bias (Greene, 2003); all parameters must be estimated simultaneously in a regression model.

Estimation of the MA coefficients,  $\{\beta_i\}$ , requires an iterative Kalman filter method which may not converge. The second, moving average summation in (6), describes a convoluting or “blurring” function, so that  $q > 1$  when the sampling interval,  $\Delta t$ , is too small.

Estimation of the MA coefficients can be avoided by decimating the time series by  $q$  to give a new time series with a larger sampling interval,  $q\Delta t$ , for which the innovation sequence,  $\{\Xi_m\}$ , is unselfcorrelated. Then (6) becomes

$$Y_m = \alpha_0 x_m + \sum_{n=1}^p \alpha_n \cdot y_{m-n} + \Xi_m \quad , \quad m = 1, \dots, M \quad (7)$$

where  $m = qi$ ,  $qM \leq N$ , The model summarized by (7) is an ARX(p) model (for ‘autoregressive with exogenous variable’). The regression coefficients,  $\alpha_i$ , and their confidence limits are estimated using Ordinary Least Squares. The sequence of residuals,  $\{\xi_m\}$ , is given by

$$\xi_m = y_m - \left( \hat{\alpha}_0 x_m + \sum_{n=1}^p \hat{\alpha}_n \cdot y_{m-n} \right) \quad , \quad m = 1, \dots, M \quad (8)$$

where  $y_m$  is the sample value or ‘realization’ of  $Y_m$  and  $\hat{\alpha}_0$  to  $\hat{\alpha}_p$  are the regression coefficient estimates. The  $\{\xi_m\}$  are tested using the  $Q$  statistic with probability  $P$  (Ljung & Box, 1978). The minimum number of coefficients,  $\hat{p}$ , is found for which  $P$  is greater than some confidence level, say 0.1, for which it can be assumed the innovation sequence is not self-correlated.

Our best estimate of the relationship between the two time series is then

$$\sum_{n=0}^{\hat{p}} \hat{\gamma}_n y_{m-n} = \hat{\alpha}_0 x_m \quad (9)$$

where

$$\hat{\gamma}_0 = 1 \quad (10)$$

and

$$\hat{\gamma}_n = -\hat{\alpha}_n \quad , \quad n = 1, \dots, \hat{p} \quad (11)$$

The sequence  $\{\gamma_n\}$  specified by (9) is the prediction error filter of the autoregressive process. (Reid, 1979).

The discrete equivalents of the continuous IRFs defined by (3) and (4) are

$$y_i = \sum_{p=0}^{\infty} I_p x_{i-p} = \alpha_0 \sum_{p=0}^{\infty} \mathfrak{S}_p x_{i-p} \quad , \quad i = 1, \dots, N \quad (12)$$

Thus, the normalized FIR,  $\mathfrak{S}$ , is the convolutional inverse of the prediction error filter  $\{\gamma_i\}$ .

The simplest regression relationship between  $y_i$  and  $x_i$  is the ARX(1) model in which  $\alpha_i \equiv 0$  for  $i > 1$ , i.e.

$$y_i = \alpha_0 x_i + \alpha_1 y_{i-1} + \xi_i \quad , \quad i = 1, \dots, N \quad (13)$$

which, by recursive substitution of  $y_i$  becomes

$$y_i = \alpha_0 \sum_{p=0}^{\infty} \alpha_1^p x_{i-p} + \sum_{p=0}^{\infty} \alpha_1^p \xi_i \quad , \quad i = 1, \dots, N \quad (14)$$

that is

$$y_i = \sum_{p=0}^{\infty} I_p x_{i-p} + \eta_i \quad , \quad i = 1, \dots, N \quad (15)$$

where  $I_p$  is the impulse response function and  $\eta_i$  is a random variable with zero mean. The prediction error filter is  $\{1, -\alpha_1\}$  which has convolutional inverse  $\{1, \alpha_1, \alpha_1^2, \dots\}$ , a geometric sequence with common ratio  $\alpha_1$ . The  $n$ th term of the IRF is given by

$$I_n = \alpha_0 \alpha_1^n = \alpha_0 \exp\left(-\frac{nq\Delta t}{\tau}\right) \quad (16)$$

and the impulse response can be regarded as discretely sampled from a continuous exponential function with time constant given by

$$\tau = -q\Delta t \ln(\hat{\alpha}_1) \quad (17)$$

Equation (15) has the form of a regression model so one may well ask, why not use it to estimate the  $I_p$  directly from the data? The reason is that (15) is not a regression model because  $\eta_i$  is the outcome of a moving average process and so is highly self-correlated. We have avoided the pitfalls of MA processes by estimating the *convolutional inverse* of the IRF rather than the IRF itself. Further discussion is given by Maillet et al. (2023).

### 4.3 Sensitivity

The sensitivity of the system,  $S$ , is defined here as the response at infinity to a unit step function,  $H_j$ , where  $H_j = 0$  for  $j < 0$  and  $H_j = 1$  for  $j \geq 0$ .

$$S = \lim_{k \rightarrow \infty} S_k = \lim_{k \rightarrow \infty} \sum_{i+j=k} I_i H_j = \sum_{k=0}^{\infty} I_k \quad (18)$$

i.e. it is the sum of the terms of the impulse response. Its estimate,  $\hat{S}$ , is a random variable on which confidence limits can be placed.

### 4.4 Application to Carbon Dioxide Concentration

The above method was applied to annual means (Meinshausen et al., 2017) of atmospheric CO<sub>2</sub> concentration,  $C_i$  as  $y_i$ , vs global fossil fuel emissions,  $E_i$  as  $x_i$ . The latter were downloaded for the interval 1850 to 2014 from the Carbon Dioxide Information Analysis Center (Boden et al., 2017).

Applying the Ljung-Box test to the residuals given by (8) for ARX(p) for  $p = 0, \dots, 5$  resulted in zero probabilities in all cases. The ARMAX method revealed a significant moving average component with  $q = 2$ . For this reason both time series were decimated by 2 and the ARX / Ljung-Box method reapplied. The results for the decimated data are shown in Table 2. The probability,  $P$ , for the ARX(1) run has a value of 0.4359 indicating that the null hypothesis that the residuals are unselfcorrelated cannot be rejected.

The estimated regression coefficients are  $\hat{\alpha}_0 = 0.21$  and  $\hat{\alpha}_1 = 0.969$  with 95 percent confidence limits 0.945 and 0.992. Substituting  $\hat{\alpha}_1$  and into (17) and multiplying by  $\ln(2)$  gives a half-time of 43 years. The normalized impulse response is shown in Figure 3 along with those of Figure 17 of MRH.

The sensitivity estimate,  $S$ , was 6.77 p.p.m.GtCO<sub>2</sub><sup>-1</sup>.year with 95 percent, t-test confidence limits of 4.03 and 20.15 p.p.m.GtCO<sub>2</sub><sup>-1</sup>.year. The probability that  $S > 10^5$  was 0.012 whereas the sensitivity of the IRF due to MRH is infinite. We can conclude that  $A_0 = 0$  in (5) implying no significant remnant fraction.

## 5 Discussion

Month by month variations in atmospheric carbon dioxide concentrations are due to the absorption and out-gassing of CO<sub>2</sub> by the mixed layer of the ocean as it is warmed and cooled by fluctuating weather systems such as El Niño.

The precise fit of the regression line in Figure 2 is in sharp contrast to the noisiness of the monthly rates of change shown Figure 1. This apparent contradiction is resolved when we consider the mixed layer Kraus & Turner (1967). The mixed layer is a turbulent layer in which winds and waves have homogenized temperature and chemistry down to some

depth which varies between about 10m and 200m. Wind stress increases the depth while solar radiation in calm conditions renews stratification. Because of its turbulent nature, the mixed layer is in intimate contact with the atmosphere, so that heat and soluble gases exchange rapidly between the two reservoirs. The highly stratified thermocline lies below the mixed layer. Apart from regions of upwelling and downwelling, heat and dissolved substances are transferred through the thermocline to and from the deep ocean largely by diffusion.

In effect then, there are three reservoirs: the atmosphere, the mixed layer and the deep ocean. At time scales of months, exchange of  $\text{CO}_2$  between the mixed layer and the atmosphere predominate whereas at time scales of years to decades, the exchange of  $\text{CO}_2$  between the deep ocean and the mixed layer predominates. At these longer time scales the mixed layer and atmosphere can be regarded as a single reservoir. The rapid variations in temperature seen in Figure 1d only involve the atmosphere and the mixed layer. On the other hand the variation in  $\Delta^{14}\text{CO}_2$  of Figure 2 is the result of the much slower rate of diffusion of  $^{14}\text{CO}_2$  from the atmosphere/mixed layer reservoir into the deep ocean.

At longer time scales, the response of the carbon dioxide concentration in the atmosphere to a perturbation in production rate is governed by a first order differential equation. Hence variations over time are smoothed by the convolution of the perturbation with the impulse response curve characterising that equation. The estimated impulse response curve is exponential with a half-time of 43 years and zero remnant fraction.

The impulse response and sensitivity of  $\text{CO}_2$  concentration estimated statistically are quite different from model-derived values. A possible explanation is the following: the real deep ocean is bounded by a turbulent mixed layer and by the highly turbulent Antarctic Circumpolar Current and will therefore be internally mixed by a Kolmogorov cascade of turbulent eddies, some with spatial scales as large as ocean basins and with time scales of, perhaps, decades. Turbulence is a stochastic phenomenon which is difficult to observe at large spatial and temporal scales and which cannot be readily emulated by deterministic models. The complexity of the eddy transports noted by Kamenkovich et al. (2021) calls for reconsideration of how they are estimated in practice, particularly in general circulation models. Eddy diffusion generated by such eddy transports would greatly increase the capacity of the deep ocean to absorb carbon dioxide and so would account for the shorter half time of the observed impulse response of atmospheric  $\text{CO}_2$  concentration.

In contrast, in numerical models the deep ocean  $\text{CO}_2$  reservoir is confined to the body water which participates in the “conveyor-belt” transport. This is a much smaller volume. In the models, the volume of the conveyor belt water becomes saturated. Alone it is insufficient to absorb all of the atmospheric  $\text{CO}_2$  with which it comes into contact and so leaves behind a remnant fraction.

## 6 Conclusion

Whatever the explanation, there is no observational evidence for the long half times and remnant fraction of atmospheric  $\text{CO}_2$  concentration predicted by numerical models of the ocean atmosphere carbon cycle. In future, the tendency of climate models to “run hot” (Hausfather et al., 2022) could well be overcome by using an empirical impulse response function such as that derived here.

## References

- Boden, T. A., Marland, G., & Andres, R. J. (2017). Global, regional, and national fossil-fuel  $\text{CO}_2$  emissions. *Carbon Dioxide Information Analysis Center, Oak Ridge National Laboratory, U.S. Department of Energy, Oak Ridge, Tenn., U.S.A.* Retrieved from <https://cdiac.ess-dive.lbl.gov/ftp/ndp030/global.1751.2014.ems> doi: 10.3334/

CDIAC/00001.V2017

- Granger, C. W. J. (1969). Investigating causal relations by econometric models and cross-spectral methods. *Econometrica*, *37*, 424-438. doi: 10.2307/1912791
- Greene, W. H. (2003). *Econometric analysis (5th ed.)*. New Jersey: Prentice Hall.
- Hamilton, E. J. (1994). *Time series analysis*. Princeton, New Jersey: Princeton University Press.
- Hausfather, Z., Marvel, K., Schmidt, G. A., Nielsen-Gammon, J., & Zelinka, M. (2022). Climate simulations: recognize the ‘hot model’ problem. *Nature*, *605*, 26-29. Retrieved from <https://www.nature.com/articles/d41586-022-01192-2> doi: <https://doi.org/10.1038/d41586-022-01192-2>
- Houghton, J. T., Ding, Y., Griggs, D. J., Noguer, M., van der Linden, P. J., Dai, X., ... Johnson, C. A. (2001). *Ipcc, 2001: climate change 2001: the scientific basis. contribution of working group 1 to the third assessment report of the intergovernmental panel on climate change*. London: Cambridge University Press.
- Kamenkovich, I., Berloff, P., Haigh, M., Sun, L., & Lu, Y. (2021). Complexity of mesoscale eddy diffusivity in the ocean. *Geophysical Research Letters*, *48*(5), e2020GL091719. Retrieved from <https://agupubs.onlinelibrary.wiley.com/doi/abs/10.1029/2020GL091719> (e2020GL091719 2020GL091719) doi: <https://doi.org/10.1029/2020GL091719>
- Kraus, E., & Turner, J. (1967). A one-dimensional model of the seasonal thermocline ii. the general theory and its consequences. *Tellus*, *19*(1), 98-106.
- Ljung, G. M., & Box, G. E. P. (1978). On a measure of a lack of fit in time series models. *Biometrika*, *65*, 297-303. doi: 10.1093/biomet/65.2.297
- Maier-Reimer, E., & Hasselmann, K. (1987). Transport and storage of co2 in the ocean - an inorganic ocean-circulation carbon cycle model. *Climate Dynamics*, *2*, 63-90. Retrieved from <https://doi.org/10.1007/BF01054491>
- Maillet, D., Zacharie, C., & Rémy, B. (2023, feb). Identification of an impulse response through a model of arx structure. *Journal of Physics: Conference Series*, *2444*(1), 012002. Retrieved from <https://dx.doi.org/10.1088/1742-6596/2444/1/012002> doi: 10.1088/1742-6596/2444/1/012002
- Meinshausen, M., Vogel, E., Nauels, A., & Lorbacher, K. (2017). Historical greenhouse gas concentrations for climate modelling (cmip6). *Geosci. Model Dev.*, *10*, 2057-2116. (<https://www.climatecollege.unimelb.edu.au/cmip6>)
- Nydal, R., & Lövseth, K. (1983). Tracing bomb 14 c in the atmosphere, 1962-1980. *Journal of Geophysical Research*, *88*, 3621-42.
- Reid, J. S. (1979). Confidence limits and maximum entropy spectra. *J. Geophys. Res.*, *84*(A9), 5289-5301.
- Riad, S. (1986). The deconvolution problem: An overview. *Proceedings of the IEEE*, *74*(1), 82-85. doi: 10.1109/PROC.1986.13407
- Siegenthaler, U., & Joos, F. (1992). Use of a simple model for studying ocean tracer distributions and the global carbon cycle. *Tellus*, *44B*(3), 186-207.
- Trenberth, K. E. (1997, 12). The definition of el niño. *Bulletin of the American Meteorological Society*, *78*(12), 2771-2778. doi: 10.1175/1520-0477(1997)078<2771:TDOENO>2.0.CO;2
- Zeebe, R. E. (2011, May). On the molecular diffusion coefficients of dissolved CO<sub>2</sub>, HCO<sub>3</sub><sup>-</sup>, and CO<sub>3</sub><sup>2-</sup> and their dependence on isotopic mass. *Geochimica et Cosmochimica Acta*, *75*(9), 2483-2498. doi: 10.1016/j.gca.2011.02.010

Statistic	Value
slope	-.06289
intercept	$-7.76 \times 10^{-15}$
$r$	-0.9939
$r^2$	0.9878
standard error	.0003395

**Table 1.** Regression Statistics

Run	Q	pvalue
C(t) vs E(t) only	513.5	0.0000
C(t) vs E(t), C(t-1)	28.5	0.4359
C(t) vs E(t), C(t-1), C(t-2)	28.6	0.3830
C(t) vs E(t) to C(t-3)	24.5	0.5483
C(t) vs E(t) to C(t-4)	24.3	0.5049
C(t) vs E(t) to C(t-5)	22.0	0.5796

**Table 2.** Ljung-Box parameter,  $Q$ , and its probability,  $P$ , for five ARX runs of CO<sub>2</sub> concentration, C, vs. global fossil fuel emissions, E. Both time series were decimated by 2.

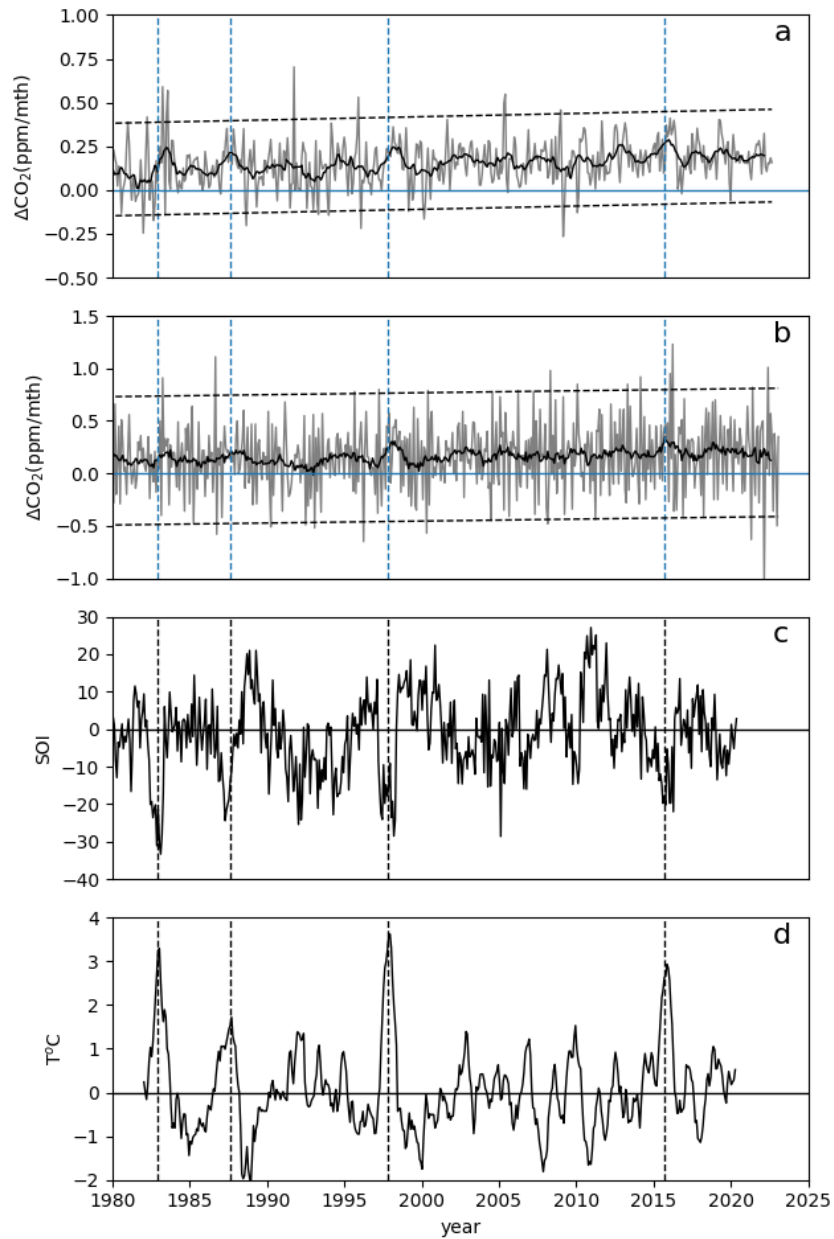


**Figure 1.** Monthly rate of change in atmospheric CO<sub>2</sub> concentration (grey) and 13 month running mean (black) at Cape Grim (a) and Mauna Loa (b). Horizontal dashed lines show  $2\sigma$  confidence limits. c. Southern Oscillation Index. d. Sea Surface Temperature anomaly of the Niño 3 region of the Equatorial Pacific. Vertical dashed lines are times of peak SST.

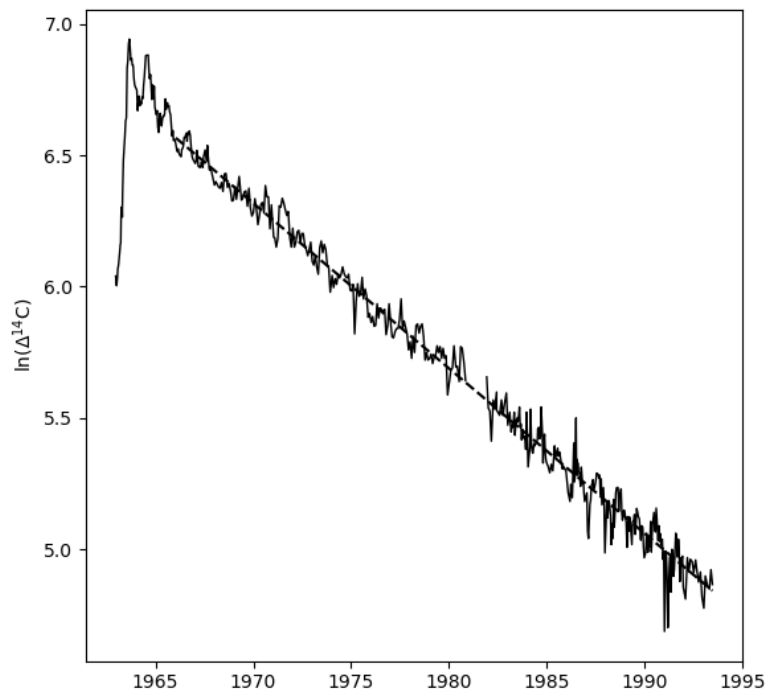


**Figure 2.** The natural logarithm of  $\Delta^{14}\text{C}$  values recorded at Fruholmen, Norway as a function of time. Dashed line: regression line fitted between January 1966 and June 1993.

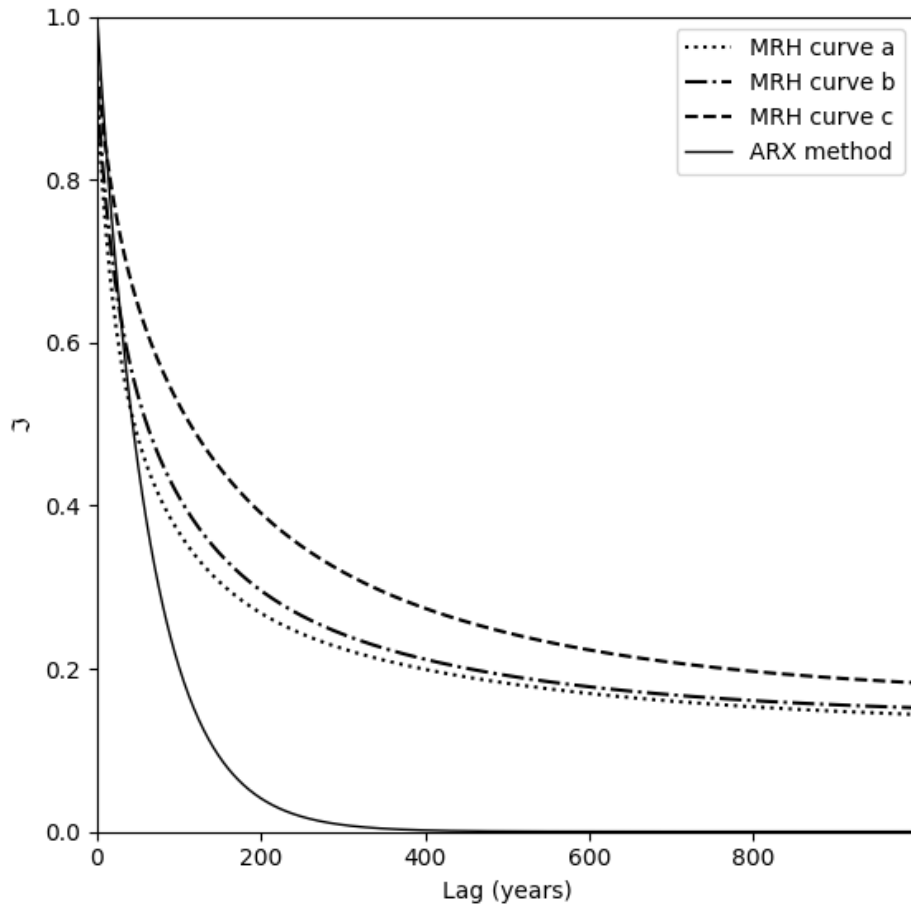


**Figure 3.** The normalized impulse response,  $\mathfrak{S}$ , of Carbon Dioxide concentration due to an impulse in CO<sub>2</sub> emissions derived from observed time series using the ARX method (solid line). Also shown are the model-derived, normalized impulse response functions corresponding to the three emissions scenarios of of Maier-Reimer & Hasselmann (1987) (broken lines).